
This is an electronic reprint of the original article.
This reprint may differ from the original in pagination and typographic detail.

Trzaskowska, A.; Hakonen, P.; Wiesner, M.; Mielcarek, S.

Generation of a mode in phononic crystal based on 1D/2D structures

Published in:
ULTRASONICS

DOI:
[10.1016/j.ultras.2020.106146](https://doi.org/10.1016/j.ultras.2020.106146)

Published: 01/08/2020

Document Version
Publisher's PDF, also known as Version of record

Published under the following license:
CC BY-NC-ND

Please cite the original version:
Trzaskowska, A., Hakonen, P., Wiesner, M., & Mielcarek, S. (2020). Generation of a mode in phononic crystal based on 1D/2D structures. *ULTRASONICS*, 106, 1-7. Article 106146.
<https://doi.org/10.1016/j.ultras.2020.106146>



Generation of a mode in phononic crystal based on 1D/2D structures

A. Trzaskowska^{a,*}, P. Hakonen^b, M. Wiesner^a, S. Mielcarek^a

^a Faculty of Physics, Adam Mickiewicz University, Uniwersytetu Poznańskiego 2, 61-614 Poznań, Poland

^b Low Temperature Laboratory, Department of Applied Physics, Aalto University, P.O. Box 15100, FI-00076 Aalto, Finland

ARTICLE INFO

Keywords:

Phononic
Surface phonons
Brillouin scattering spectroscopy
Finite Element Method

ABSTRACT

The modification of phononic crystals by surface structuring allows obtaining a new parameter describing the dynamics of the structure produced in this way. We have investigated the dispersion relation of surface acoustic waves propagating in a phononic material which is based on nanometer-scale surface modulation using interconnected one-dimensional array of stripes and a two-dimensional array of pillars. The influence of these two array components on the dispersion relation has been determined experimentally (Brillouin light scattering) and theoretically (Finite Element Method). The interaction of these two nanostructures supports a new mode which is not observed in independent structures of pillars and stripes. The influence of the relative position of these two nanostructures on the frequency of the new mode has been determined.

1. Introduction

Phononic crystals are special periodic materials with great promise for controlling and manipulating the propagation of elastic waves. The periodic nature of such materials gives them novel properties that cannot be found in bulk materials such as, for example, near zero group velocity or formation of band gap – the range of frequency where the acoustic waves cannot propagate [1–7]. A defect free phononic crystals are very useful in actual fabrication at the nanoscale because can strongly reduce tedious technological processes and potentially improve the precision of the devices [8]. The addition of defects to phononic crystals (for example, local irregularity of the phononic lattice) provides possibilities to create new devices to control acoustic wave transmission [9–13]. The idea of applying an additional layer to the fragment of the phononic structure allows the evolution of the bandgap and localization of the own vibrations of the pillars [14]. The modulation of elastic properties and the dimension of nanostructures give further opportunities to influence the wave propagation [15–19]. Moreover, many recent studies have addressed phononic crystals with regard to their applications. Such materials can be useful in communication, sensing, and optomechanics [20–25].

This article presents results on propagation of surface acoustic waves (SAW) in a nano-engineered phononic system consisting of one-dimensional (1D) and two-dimensional (2D) phononic structures. Each of these structures has a different location that characterizes its bandgap. Creating two structures of different dimensions in one technological process but using the same material seems to be another good

step in expanding the application possibilities of phononic materials. We used non-destructive testing methods for our research.

The Brillouin scattering of light was used for determination of the SAW dispersion relation. Theoretical calculations of the expected dispersion relation have been done using the finite element method (FEM). The main goal of our study was to determine the influence of both 1D and 2D structures – pillars and stripes – on the dispersion relation of surface acoustic waves in a phononic crystal consisting of these nanostructures as well as determining the nature of the vibrations arising at the interface of these two nanostructures.

2. Materials and methods

2.1. The samples

The naturally oxidized (0 0 1) surface of a pure Si wafer was used as the substrate. The sample was cut into chips of the size of $5 \times 5 \text{ mm}^2$ and coated with a 250 nm thick PMMA layer. Several patterns covering $100 \times 100 \mu\text{m}^2$ were fabricated on each chip using e-beam lithography (JEOL 7100F instrument). After development in MIBK solution, the chips were coated with Al in an UHV evaporator at the speed of 0.3 nm/s. The thickness of the metal on the chip was controlled by a thickness monitor with a resolution of 0.1 nm. After evaporation, the chips were subject to a lift-off and cleaning process. The resulting periodic nanostructure consisted of strongly interconnected aluminum stripes and pillars. A scanning electron micrograph of a typical sample used in our experiment is shown in Fig. 1a. The shape and parameters of stripes and

* Corresponding author.

E-mail address: olatrzas@amu.edu.pl (A. Trzaskowska).

<https://doi.org/10.1016/j.ultras.2020.106146>

Received 11 September 2019; Received in revised form 21 March 2020; Accepted 23 March 2020

Available online 07 April 2020

0041-624X/ © 2020 The Author(s). Published by Elsevier B.V. This is an open access article under the CC BY-NC-ND license (<http://creativecommons.org/licenses/by-nc-nd/4.0/>).

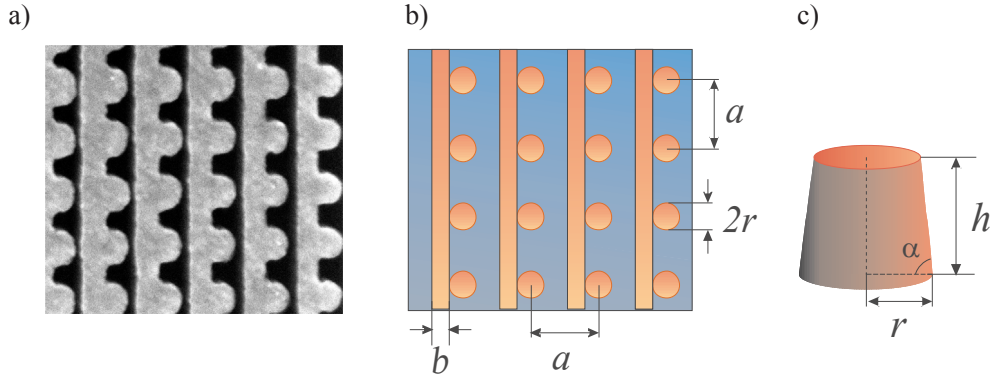


Fig. 1. Scanning electron microscope (SEM) image of aluminum nanostructure consisting of interconnected aluminum stripes and pillars deposited on a silicon substrate (a). Schematic representation of the studied phononic crystal (b, c).

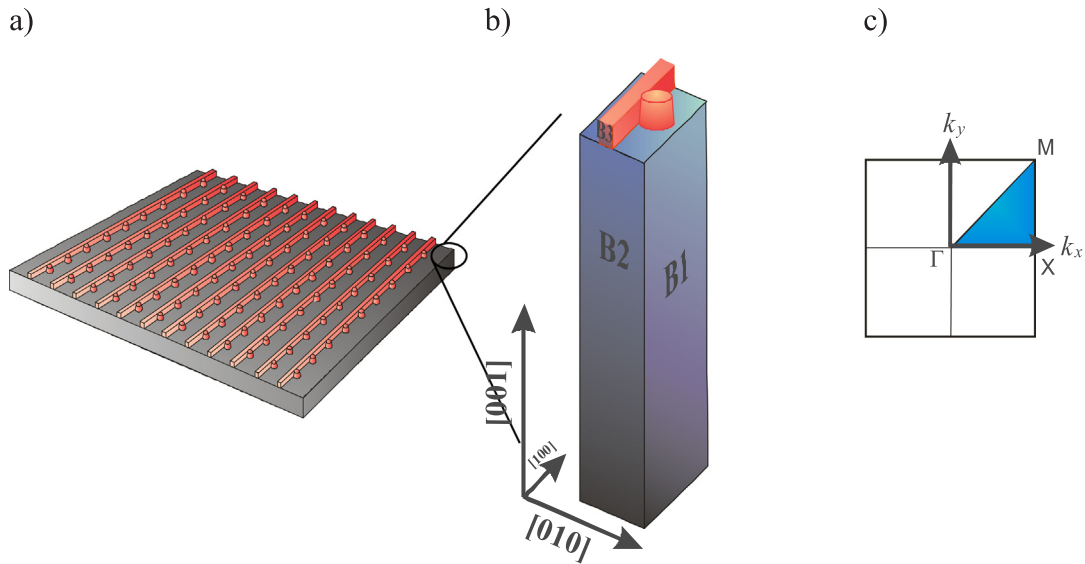


Fig. 2. Periodic structure made of a array of pillars and stripes on Si substrate surface (a). Schematic view of the unit cell used in FEM simulations (b). The irreducible first Brillouin zone of the square lattice (c).

pillars (Fig. 1) were defined by using SEM and AFM imaging: the width of the stripes $b = 135$ nm, the radius of the pillar $r = 105$ nm, the tilting angle of the wall of the pillar $\alpha = 3.8$ degrees (i.e. more precisely the pillars were truncated cones Fig. 1c). The height of the aluminum nanostructure was $h = 160$ nm. The structures shown in Fig. 1 are characterized by the lattice constant of $a = 500$ nm, which was the same for both the stripes and the pillars. The stripes orientation with respect to the silicon lattice is shown in Fig. 2b.

2.2. Experimental setup

The propagation of surface acoustic waves along the silicon surfaces covered with an aluminum nanostructure was studied using a six-pass, tandem Brillouin spectrometer (JRS Scientific Instruments) which ensures a contrast of 10^{10} [26–27]. The source of light was a 200 mW Nd:YAG single-mode diode-pumped laser, emitting the second harmonics of light of the length $\lambda_0 = 532$ nm (Excelsior Spectra Physics). A detailed description of the experimental setup is found in Refs. [28,29]. Measurements were made in the backscattering geometry. The incident light was polarized in the sagittal plane defined by the wave vector of a given phonon and the normal to the sample surface. The SAW energy is represented by the Brillouin frequency shift Δf of the inelastically scattered laser beam. The range of wavelengths of the Rayleigh SAW studied was from about 280 nm to 7000 nm [30].

Owing to its high sensitivity, Brillouin spectroscopy permits detailed investigations of the dispersion relation of SAW propagating in the patterned 1D/2D aluminum structures.

3. FEM simulations

The dispersion relation for surface acoustic waves propagating in the studied phononic crystal was simulated using the finite element method code of COMSOL Multiphysics [31]. Phononic crystal with strong interconnected aluminum stripes and pillars on silicon substrate is schematically shown in Fig. 2a. The elementary cell used in the FEM simulation is displayed in Fig. 2b. Pillars form a square lattice which is described by 2D irreducible Brillouin zone of the square lattice which is given in Fig. 2c.

The silicon substrate was treated as a uniform semispace $z \leq 0$ with nanostructures on the top of semispace. For simulations, the substrate was taken as strictly flat. The calculations were performed for the elastic constants of cubic silicon $c_{11} = 165.7$ GPa, $c_{12} = 63.9$ GPa, $c_{44} = 79.9$ GPa and density $\rho_{Si} = 2331$ kg·m⁻³ [32], aluminum $c_{11} = 111.3$ GPa, $c_{12} = 59.1$ GPa, and density $\rho_{Al} = 2700$ kg·m⁻³ [33]. The geometrical parameters used during the simulations corresponded to the real parameters of the experimentally investigated sample. Bloch – Floquet periodic boundary conditions were applied to walls B1, B2 and B3 (Fig. 2b), and the opposite walls parallel to them. Fixed

boundary condition was applied to the bottom surface of the unit cell. The height of the elementary cell used in the simulations was correlated with the wavelength of the acoustic wave propagating in the sample.

4. Results

The investigated phononic structure is complex in terms of the construction. In the studied samples, the phononic structure consisted of parallel lines, i.e. stripes (one-dimensional phononic crystal, 1DPnC) and pillars (two-dimensional phononic crystal, 2D PnC) which are coupled (1D/2D double-lattice PnC). The pillars structure forms a 2D square lattice. Therefore, the experimental investigations of SAW propagation was done in two different directions marked in the irreducible first Brillouin zone of the square lattice as k_x and k_y (Fig. 2c). In the first measurements, the direction of the SAW wave vector q was along the stripes which correspond to the k_x direction, while in the second case, the direction of the SAW wave vector q was perpendicular to the patterned lines which correspond to the k_y direction.

From the point of view of 2D pillar array, the dispersion relations measured in the directions k_x and k_y do not differ from each other, however, for 1D stripe array, the difference is fundamental [34].

The measurements and simulations on the dispersion relation of surface acoustic waves presented in Fig. 3 for our 1D/2D double-lattice sample have been done in k_x direction (the direction of SAW propagation is along the lines of stripes). The blue dotted line in the figure corresponds to the bulk transverse wave propagates in pure silicon substrate. The brown dashed line corresponds to Rayleigh SAW propagates in pure silicon substrate. The letters A-E denote individual dispersion branches for SAW and the corresponding maps of unit cell deformation.

Even though the investigations were done for the SAW propagation along the Al stripes, the dispersion relation is typical of a 2D PnC as the dispersion relation shows the characteristic Brillouin zone folding. Typical dispersion relation of SAW for 1D PnC composed of stripes is not periodic when the waves propagate along the stripes [34]. Our result means that even a slight periodic inhomogeneity of a striped configuration (in our case it is made by a pillar connected to the stripe) induces the typical 2D PnC character of the dispersion relation in contrast to the dispersion relation observed in the 1D PnC composed of stripes alone [30]. Therefore, it can be explicitly stated that the

observed folding effect at the boundary of Brillouin zones in the dispersion relation of Fig. 3 is exclusively caused by the 2D phononic pillar lattice. The acquisition of a part of the deformation energy through the striped lattice via the pillar-line coupling results in a reduction of the frequency of each band in the dispersion relation for combined stripe and pillar phononic lattice, distinct from the bands visible in the dispersion relation characteristic to pure pillar lattices [35–36].

The obtained dispersion relation shows the existence of a non-dispersive mode A (breathing mode [37–40]) with a frequency of 4.9 GHz. The mode at frequency of 4.4 GHz (at $q = 0.0063 \text{ nm}^{-1}$) marked as B in Fig. 3 is typical of Rayleigh surface acoustic waves. The modes associated with the lowest three branches (C, D, E) of the dispersion relation can be classified as eigenmodes of the stripe/pillar lattice. As can be seen from the presented map of unit cell deformation, the strain caused by the SAW occurs both in the Al line and in the pillar.

The dispersion relation obtained for 1D/2D PnC in the k_y direction -which is the direction of the SAW propagation perpendicular to the stripes, is displayed in Fig. 4. The blue dotted line in the figure corresponds to the bulk transverse wave propagating in pure silicon substrate. The brown dashed line corresponds to Rayleigh SAW propagating in pure silicon substrate. The letters A-G denote individual dispersion branches and the corresponding maps of unit cell deformation.

The dispersion relation for SAWs propagating perpendicular to the stripes (Fig. 4) is significantly different from the dispersion relation presented in Fig. 3. Both the stripe and pillar lattices have an influence on the appearance of the folding effect in the dispersion relation. The non-dispersive modes visible in the dispersion relation are classified by 3D maps of unit cell deformation in Fig. 4 as modes A–C. The energy of each mode, as in the parallel-propagation measurement geometry, spreads over both stripes and pillars. The maps of unit cell deformation related to the dispersive eigenmodes of the phononic lattice are shown in Fig. 4 as modes D–G.

5. Discussion

The obtained characteristic dispersion relations in two different measurement geometries (along and perpendicular to the stripe structures) allow us to determine the character of the individual surface acoustic modes of each substructure of the unit cell (pillar and stripe),

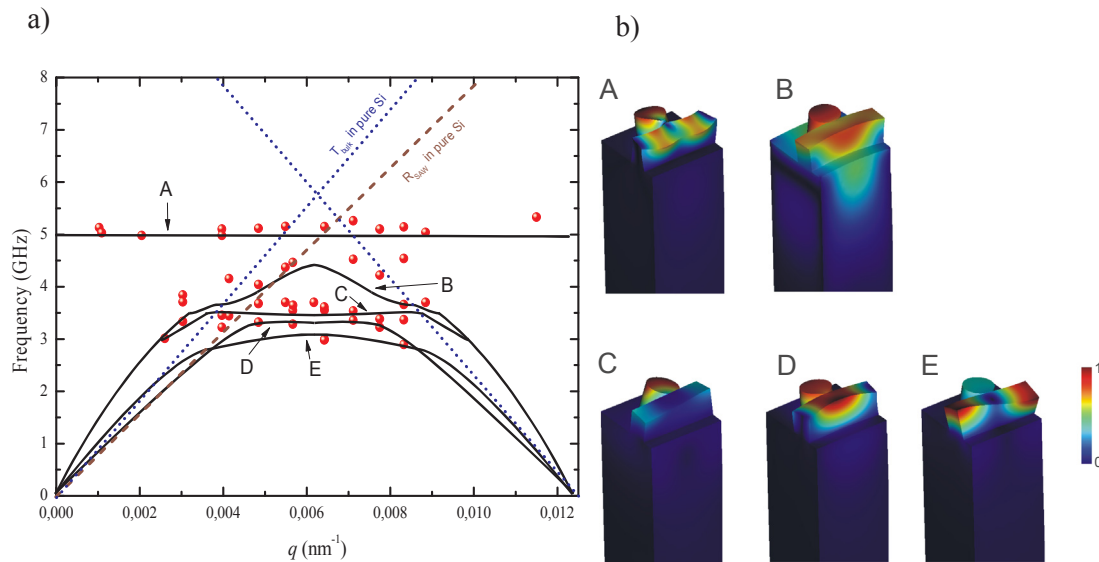


Fig. 3. Dispersion relation obtained using FEM (black lines) and BLS (red circles) for 1D/2D PnC consisting of both stripes and pillars in k_x direction (along the stripes), (waves propagate in pure silicon substrate: blue dotted line - bulk transverse wave; brown dashed line - Rayleigh SAW) (a) and 3D maps of unit cell deformation caused by the SAW at $q = 0.0063 \text{ nm}^{-1}$ (b). (For interpretation of the references to colour in this figure legend, the reader is referred to the web version of this article.)

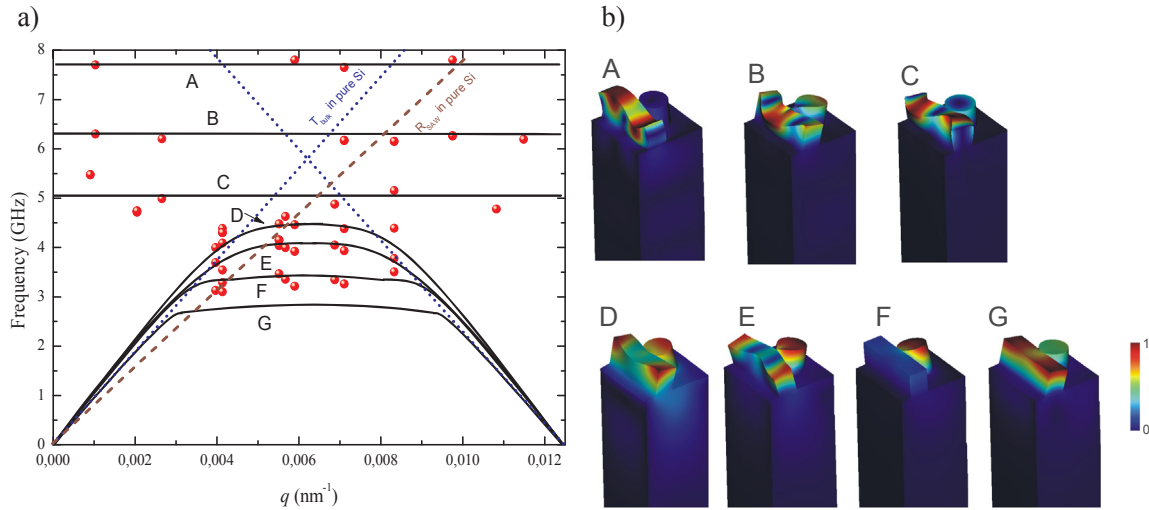


Fig. 4. Dispersion relation obtained using FEM (black lines) and BLS (red circles) for 1D/2D PnC consisting of both stripes and pillars in k_y direction (perpendicular to the stripes) (waves propagate in pure silicon substrate: blue dotted line - bulk transverse wave; brown dashed line - Rayleigh SAW) (a). 3D maps of unit cell deformation caused by the SAW at $q = 0.0063 \text{ nm}^{-1}$ (b). (For interpretation of the references to colour in this figure legend, the reader is referred to the web version of this article.)

as well as the impact of individual phononic lattices (stripes and pillars) on the propagation of the SAW. In the two studied geometries with combined stripe and pillar lattices, the frequency of bands in the dispersion relation is reduced with respect to pure lattices containing only stripes or pillars, respectively. For the two studied geometries a number of bands for a lattice combining pillars and stripes is reduced when comparing to a number of bands of each substructure separately. It is a result of coupling between two substructures: pillars and stripes.

In both studied orientations of the double-lattice sample, there are breathing modes emerging in the dispersion relation at the frequencies of 4.9 GHz (Fig. 3 mode A), 5.1, 6.3 and 7.6 GHz (Fig. 4. modes A, B, C), respectively. In the first studied orientation of the sample, the breathing mode at frequency of 4.9 GHz in Fig. 3 originates from the pillar lattice vibrations [20,37]. The breathing mode, even though initially associated with the pillar lattice only, propagates also in the lattice of stripes.

In a striped 1D PnC only guided waves can propagate. However, by connecting a stripe with a pillar, the stripe absorbs part of the deformation associated with the breathing mode of the pillar. The presence of the breathing mode, the appearance of the folding effect in the dispersion relation (Fig. 3), all together unequivocally confirm the dominant influence of the pillar phononic lattice on the propagation of surface acoustic waves in studied nanostructures when the surface waves propagate along stripes.

A more complex situation for the breathing modes occurs in the dispersion relation obtained for the SAW propagating perpendicularly to the stripe substructure (Fig. 4). The breathing mode frequency of approx. 5.1 GHz (mode C in Fig. 4) appears both on the pillar and the stripe lattices. The breathing mode at frequency of 7.6 GHz (mode A in Fig. 4) is a mode characteristic to the stripe lattice, as the 3D map of deformation shows that all energy is concentrated in the stripe. A new mode is the breathing mode at the frequency of 6.3 GHz (mode B in Fig. 4). The center of deformation associated with this mode is exactly at the connection between the stripe and the pillar. The frequency of this mode strongly depends on distance between center of the pillar and the center of the stripe. In the situation, when the pillar just touches the stripe, the distance is about 173 nm (the sum of half the width of the stripe and the radius of the pillar). Dispersion relations calculated for various distances between these sub-structures have shown that the new breathing mode appears when the pillar and the stripe are touching (Fig. 5). This figure is divided into three areas: the first and the third is the region when pillar and stripe are not connected, the second

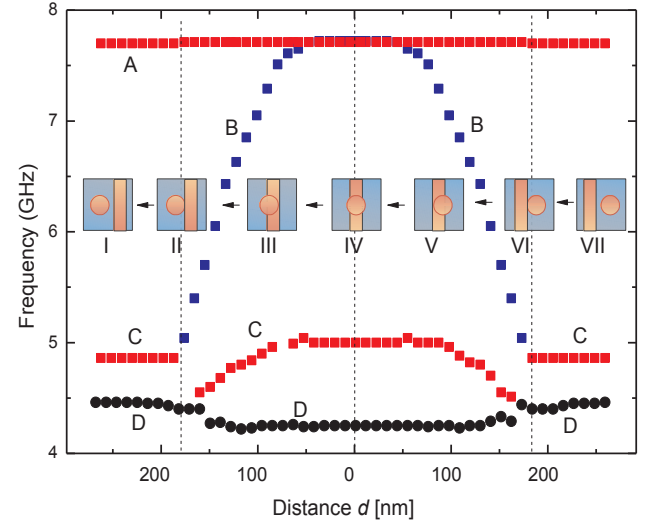


Fig. 5. Dependence between frequencies of breathing modes as a function of the distance between a pillars and a stripes. The x axis shows the distance between the centres of the pillar and the stripe. Inserts (I-VII) represent schematic orientation of pillars vs. stripes.

– when they are connected.

The breathing mode at frequency of 7.6 GHz (mode A in Figs. 4 and 5), which is characteristic to the stripe lattice, is independent on distance between stripe and pillars. The new mode B exists only for a structure consisting of coupled pillars and stripes. The frequency of the mode B strongly depends on distance between both substructures - Fig. 6.

The next mode C is typical pillar's breathing mode. It means that all the energy is mainly concentrated in the pillar which is visible in the 3D maps of the unit cell deformation in region I in Fig. 6. When the pillar and the stripe overlap in a such way that part of the pillar protrudes on both sides of the stripe (region IV in Fig. 6) the frequency of mode B is the same as the frequency of mode A, so the energy deformation is concentrated in the stripe. The most interesting situation is when the pillars and the stripes are partly connected (region II and III in Fig. 6). The frequency of this new mode B is different from the point when the pillar and the stripe are connected to the point when the pillar overlaps the stripe but it is still partly visible on one side of the stripe. In this

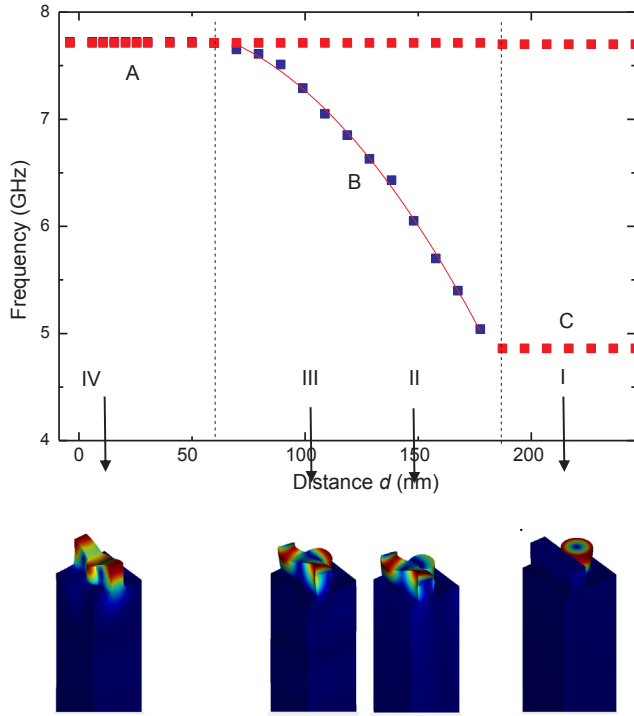


Fig. 6. Dependence between the frequency of a new breathing mode B according to the distance between a pillars and a stripes. 3D maps show deformations of the unit cell caused by the SAW at $q = 0.0063 \text{ nm}^{-1}$. Red line shows parabolic fit for mode B. (For interpretation of the references to colour in this figure legend, the reader is referred to the web version of this article.)

region the deformation energy of mode B is distracted into both the pillar and the stripe. In the region of connection between pillars and stripes the frequency of mode B is changed according to the distance between the centers of stripes and pillars. The last mode, mode D, visible in Fig. 5, is a pure Rayleigh surface acoustic wave. The frequency of this mode is decreased when the pillar and the stripe are connected. We have to remember that Rayleigh SAW propagates into all the sample, as constraints to the breathing modes in which energy is strongly concentrated in the phononic structure. The deformation energy of the Rayleigh SAW is not so sensitive to the changes of the position of the pillar and the stripe.

Observed in our experiments additional mode results from interaction between pillars and stripes. To describe strength of the interaction we introduced the filling factor f . In general definition comprise a common area of the pillar and stripe divided by the total area of a unit cell:

$$f = \frac{\text{area}_{\text{nanostructures}}}{\text{area}_{\text{unit cell}}} \quad (1)$$

The common area is related with a distance d between center of the pillar and the center of the stripe the equation for filling factor is different. When distance d fulfills a relation $0 \leq d \leq r - \frac{b}{2}$ (see Fig. 5V), the pillar resides in middle of the stripe. In this case the general definition of the filling factor takes a form:

$$f = \frac{\text{area}_{\text{stripe}} + \text{area}_{\text{two parts of the pillar}}}{\text{area}_{\text{unit cell}}} \quad (2)$$

and after development:

$$f = \frac{a \cdot b + \left[\frac{\Pi \cdot r^2 \cdot 2 \cdot \cos^{-1}\left(\frac{\frac{b}{2} + d}{r}\right)}{360^\circ} - \frac{r^2 \sin\left[2 \cdot \cos^{-1}\left(\frac{\frac{b}{2} + d}{r}\right)\right]}{2} \right] + \left[\frac{\Pi \cdot r^2 \cdot 2 \cdot \cos^{-1}\left(\frac{\frac{b}{2} - d}{r}\right)}{360^\circ} - \frac{r^2 \sin\left[2 \cdot \cos^{-1}\left(\frac{\frac{b}{2} - d}{r}\right)\right]}{2} \right]}{a^2}$$

Curly bracket refers to the areas of the pillar which are on both (right and left) side on the stripe.

When the part of the pillar partially overlaps a stripe (but not more than half of pillar), so the distance d fulfills following relation $(r - \frac{b}{2} \leq d \leq \frac{b}{2})$ (see Fig. 5III, V) the filling factor is defined as:

$$f = \frac{\text{area}_{\text{stripe}} + \text{area}_{\text{one part of the pillar}}}{\text{area}_{\text{unit cell}}} \quad (3)$$

and after development:

$$f = \frac{a \cdot b + \left[\frac{\Pi \cdot r^2 \cdot 2 \cdot \cos^{-1}\left(\frac{\frac{b}{2} - d}{r}\right)}{360^\circ} - \frac{r^2 \sin\left[2 \cdot \cos^{-1}\left(\frac{\frac{b}{2} - d}{r}\right)\right]}{2} \right]}{a^2}$$

If part of pillar partially overlaps the stripe (more than half of the pillar), so the distance d fulfill the following relation $(\frac{b}{2} \leq d \leq r)$ (see Fig. 5IV, VI) the fill factor has a form:

$$f = \frac{a \cdot b + \left[\frac{\Pi \cdot r^2 \cdot 2 \cdot \cos^{-1}\left(\frac{\frac{b}{2} - d}{r}\right)}{360^\circ} + \frac{r^2 \sin\left[2 \cdot \cos^{-1}\left(\frac{\frac{b}{2} - d}{r}\right)\right]}{2} \right]}{a^2}$$

Because pillar and stripe cannot be connected so the f factor is defined as:

$$f = \frac{\text{area}_{\text{stripe}} + \text{area}_{\text{pillar}}}{\text{area}_{\text{unit cell}}} \quad (4)$$

and after development:

$$f = \frac{a \cdot b + \Pi \cdot r^2}{a^2}$$

Depending on the mutual position of pillar and stripe for the investigated sample the filling factor ranges from 0.31 to 0.41. Deformation of unit cell caused by the SAW is different for different f factor (Table 1).

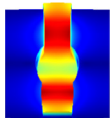
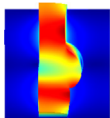
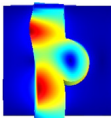
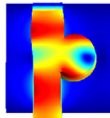
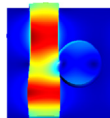
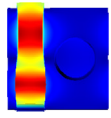
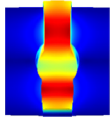
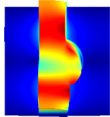
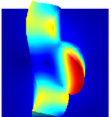
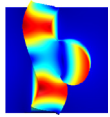
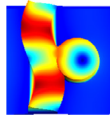

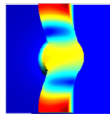
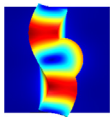
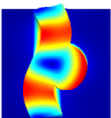
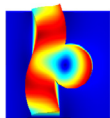
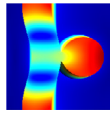
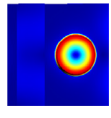
Presented above comparison of deformation for several filling factor show concentration of the A and C modes into the stripe and pillar respectively for separated pillars and stripes. The deformation related with a new breathing mode B exists only in structure consisting of connected pillars and stripes. The frequency of this mode is quadratic function of the filling factor f (see Fig. 6. red line).

6. Conclusions

The result of our experiments revealed an effect of coupling between 1D and 2D sublattices on the dispersion relations of a complex structure consisting of both substructures. We find that, if the system consists of 1D and 2D phononic sublattices, the dispersion relation is typical for a 2D lattice. Thus, the dispersion relation is always typical for the more

Table 1

2D deformations of the unit cell caused by the SAW of phononic crystal for three breathing modes for different filling factor.

	Filling factor					
	0.310	0.318	0.351	0.383	0.407	0.410
mode A 7.71 GHz						
mode B 7.71 GHz						
	7.71 GHz	7.65 GHz	7.05 GHz	6.05 GHz	5.04 GHz	
mode C 5 GHz						
	5 GHz	5 GHz	4.96 GHz	4.7 GHz	4.44 GHz	5 GHz

complex structure - in our case, the 2D pillar-based phononic structure. The 1D lattice, in our case a lattice of stripes, affects the frequency of the modes in the dispersion relation. In addition, the breathing modes occurring in the lattices of stripes or pillars are also present in the studied phononic double-lattice of stripes and pillars. The basic breathing modes observed in the studied nanostructures exist both in the stripe and pillar lattices, indicating that these modes are independent of each other. It is remarkable that the combined system of stripes and pillars generates also a new breathing mode (cf. Fig. 56), where the deformation field of the mode is concentrated in the coupling region between stripes and pillars.

Finally, it can be concluded that the formation of phononic crystals based on lattices of various dimensions, in our work 1D and 2D lattices, provides the possibility to produce a kind of generator for modes of frequencies differing from frequencies characteristic for uncoupled 1D and 2D substructures. Such a generator, moreover, will fulfill its function only in a particular direction of wave propagation. Phononic crystals have diverse application potentials in many fields and the modulation of wave propagation, tunable and active manipulation of waves have outlining future directions in the application of phononics materials [41].

Declaration of Competing Interest

The authors declare that they have no known competing financial interests or personal relationships that could have appeared to influence the work reported in this paper.

Acknowledgment

We acknowledge the financial assistance from Polish National Science Center under grant no. UMO-2016/21/B/ST3/00452.

The work of PJH was supported by the Academy of Finland projects 314448 (BOLOSE) and 312295 (CoE, Quantum Technology Finland). This research project utilized the Aalto University OtaNano/LTL infrastructure which is part of European Microkelvin Platform.

References

- [1] T. Gorishnyy, C.K. Ullal, M. Maldovan, G. Fytas, E.L. Thomas, Hypersonic phononic crystals, *Phys. Rev. Lett.* 94 (2005) 115501, <https://doi.org/10.1103/PhysRevLett.94.115501>.
- [2] A. Khelif, Y. Achaoui, S. Benchabane, V. Laude, B. Aoubiza, Locally resonant surface acoustic wave band gaps in a two-dimensional phononic crystal of pillars on a surface, *Phys. Rev. B* 81 (2010) 214303, <https://doi.org/10.1103/PhysRevB.81.214303>.
- [3] Y. Achaoui, A. Khelif, S. Benchabane, L. Robert, V. Laude, Experimental observation of locally-resonant and Bragg band gaps for surface guided waves in a phononic crystal of pillars, *Phys. Rev. B* 83 (2011) 104201, <https://doi.org/10.1103/PhysRevB.83.104201>.
- [4] M. Badreddine Assouarand, M. Oudich, Dispersion curves of surface acoustic waves in a two-dimensional phononic crystal, *Appl. Phys. Lett.* 99 123505 (2011), <https://doi.org/10.1063/1.3626853>.
- [5] M. Torres, F.R. Montero de Espinoza, Ultrasonic band gaps and negative refraction, *Ultrasonics* 42 (2004) 787–790, <https://doi.org/10.1016/j.ultras.2004.01.041>.
- [6] V. Laude, M. Wilm, S. Benchabane, A. Khelif, Full band gap for surface acoustic waves in a piezoelectric phononic crystal, *Phys. Rev. E* 71 (2005) 036607, <https://doi.org/10.1103/PhysRevE.71.036607>.
- [7] Y. Guo, D. Brick, M. Grossmann, M. Hettich, T. Dekorsy, Acoustic beam splitting at low GHz frequencies in a defect-free phononic crystal, *Appl. Phys. Lett.* 110 (2017) 031904, <https://doi.org/10.1063/1.4974491>.
- [8] V. Laude, *Phononic crystals: artificial crystals for sonic, acoustic, and elastic waves*, De Gruyter Stud. Math. Phys. (2015).
- [9] R.H. Olsson, I. El-Kady, Microfabricated phononic crystal devices and applications, *Meas. Sci. Technol.* 20 (2009) 012002, <https://doi.org/10.1088/0957-0233/20/1/012002>.
- [10] Z.-G. Huang, Silicon-based filters, resonators and acoustic channels with phononic crystal structures, *J. Phys. D: Appl. Phys.* 44 (2011) 245406, <https://doi.org/10.1088/0022-3727/44/24/245406>.
- [11] Y. Pennec, J.O. Vasseur, B. Djafari-Rouhani, L. Dobrzynski, P.A. Deymier, Two-dimensional phononic crystals: Examples and applications, *Surf. Sci. Rep.* 65 (2010) 229–291, <https://doi.org/10.1016/j.surfrep.2010.08.002>.
- [12] E. Coffy, S. Euphrasie, M. Addouche, P. Vairac, A. Khelif, Evidence of a broadband gap in a phononic crystal strip, *Ultrasonics* 78 (2017) 51–56, <https://doi.org/10.1016/j.ultras.2017.03.003>.
- [13] E. Muzar, J.A.H. Stotz, Surface acoustic wave modes in two-dimensional shallow void inclusion phononic crystals on GaAs, *J. Appl. Phys.* 126 (2019) 025104, <https://doi.org/10.1063/1.5056311>.
- [14] M. Moutaouekkil, A. Talbi, E.H. El Boudouti, O. Elmazria, B. Djafari-Rouhani, P. Pernod, O. BouMatar, Highly confined radial contour modes in phononic crystal plate based on pillars with cap layers, *J. Appl. Phys.* 126 (2019) 055101, <https://doi.org/10.1063/1.5099956>.
- [15] M. Oudich, M. Badreddine Assouar, Surface acoustic wave band gaps in a diamond-based two-dimensional locally resonant phononic crystal for high frequency applications, *J. Appl. Phys.* 111 (2012) 014504, <https://doi.org/10.1063/1.3673874>.
- [16] Liu Zong-Fa, Wu Bin, He Cun-Fu, The properties of optimal two-dimensional phononic crystals with different material contrasts, *Smart Mater. Struct.* 25 (2016) 095036, <https://doi.org/10.1088/0964-1726/25/9/095036>.
- [17] M. Maldovan, Sound and heat revolutions in phononics, *Nature* 503 (2013) 209–217, <https://doi.org/10.1038/nature12608>.
- [18] Y. Guo, M. Schubert, T. Dekorsy, Finite element analysis of surface modes in phononic crystal waveguides, *J. Appl. Phys.* 119 (2016) 124302, <https://doi.org/10.1063/1.4944804>.
- [19] Y.F. Li, F. Meng, S. Li, B. Jia, S. Zhou, X. Huang, Designing broad phononic band gap for in-plane modes, *Phys. Lett. A* 382 (2018) 679–684, <https://doi.org/10.1016/j.physleta.2017.12.050>.
- [20] H. Shin, J.A. Cox, R. Jarecki, A. Starbuck, Z. Wang, P.T. Rakich, Control of coherent

- information via on-chip photonic–phononic emitter–receivers, *Nat. Commun.* 6 (2015) 6427, <https://doi.org/10.1038/ncomms7427>.
- [21] K. Rostem, D.T. Chuss, K.L. Denis, E.J. Wollack, Wide-stopband aperiodic phononic filters, *J. Phys. D: Appl. Phys.* 49 (2016) 255301, <https://doi.org/10.1088/0022-3727/49/25/255301>.
- [22] G. Fuxi, W. Yang, *Data Storage at the Nanoscale: Advances and Application*, Taylor & Francis, 2015.
- [23] S. Volz, J. Ordóñez-Miranda, A. Shchepetov, M. Prunnila, J. Ahopelto, T. Pezeril, G. Vaudel, V. Gusev, P. Ruello, E.M. Weig, M. Schubert, M. Hettich, M. Grossman, T. Dekorsy, F. Alzina, B. Graczykowski, E. Chavez-Angel, J.S. Reparaz, M.R. Wagner, C.M. Sotomayor-Torres, S. Xiong, S. Neogi, D. Donadio, Nanophononics: state of the art and perspectives, *EPJ B* 89 (2016) 15, <https://doi.org/10.1140/epjb/e2015-60727-7>.
- [24] J. Gomis-Bresco, D. Navarro-Urrios, M. Oudich, S. El-Jallal, A. Griol, D. Puerto, E. Chavez, Y. Pennec, B. Djafari-Rouhani, F. Alzina, A. Martinez, C. Sotomayor-Torres, A one-dimensional optomechanical crystal with a complete phononic band gap, *Nat. Commun.* 5 (2014) 4452, <https://doi.org/10.1038/ncomms5452>.
- [25] T. Roy, S. Zhang, I.W. Jung, M. Troccoli, F. Capasso, D. Lopez, Dynamic metasurface lens based on MEMS technology, *APL Photon.* 3 (2018) 021302, <https://doi.org/10.1063/1.5018865>.
- [26] J.R. Sandercock, *Trends in Brillouin Scattering: Studies of Opaque Materials, Supported Films and Central Modes*, Topics in Applied Physics vol. 51, (1982) 173–206.
- [27] A.G. Every, Measurement of the near-surface elastic properties of solids and thin supported films, *Meas. Sci. Technol.* 13 (2002) R21–R39, <https://doi.org/10.1088/0957-0233/13/5/201>.
- [28] S. Mielcarek, A. Trzaskowska, B. Mroz, T. Andrews, High resolution Brillouin scattering studies of beta $\text{Gd}_2(\text{MoO}_4)_3$; the bulk and surface phase transitions, *J. Phys.: Condens. Matter* 17 (2005) 587–598, <https://doi.org/10.1088/0953-8984/17/4/003>.
- [29] A. Trzaskowska, S. Mielcarek, B. Graczykowski, F. Stobiecki, Surface waves investigation in NiFe/Au/Co/Au multilayers by high-resolution Brillouin spectroscopy, *J. Alloys Comp.* 517 (2012) 132–138, <https://doi.org/10.1016/j.jallcom.2011.12.059>.
- [30] A. Trzaskowska, S. Mielcarek, M. Wiesner, One-dimensional modulation of the stripe in a surface phononic lattice: The effect on propagation of surface waves, *J. Appl. Phys.* 116 (2014) 214303, <https://doi.org/10.1063/1.4902894>.
- [31] COMSOL Multiphysics finite element software, COMSOLAB, Sweden.
- [32] G.W. Farnell, Properties of elastic surface waves, in: W.P. Mason, R.N. Thurston, (Eds.), *Physical Acoustics*, vol. 6, Academic Press, New York, 1970, p. 109–166.
- [33] G.W. Farnell, E.L. Adler, Elastic wave propagation in thin layers, in: W.P. Mason, R. N. Thurston, (Eds.), *Physical Acoustics* vol. 9, Academic Press, New York, 1972, 35–128.
- [34] B. Graczykowski, M. Sledzinska, N. Kehagias, F. Alzina, J.S. Reparaz, C.M. Sotomayor-Torres, Hypersonic phonon propagation in one-dimensional surface phononic crystal, *Appl. Phys. Lett.* 104 (2014) 123108, <https://doi.org/10.1063/1.4870045>.
- [35] C. Ma, J. Guo, Y. Liu, Extending and lowering band gaps in one-dimensional phononic crystal strip with pillars and holes, *J. Phys. Chem. Sol.* 87 (2015) 95–103, <https://doi.org/10.1016/j.jpcs.2015.07.008>.
- [36] C. Sumanya, J.D. Comins, A.G. Every, Surface Brillouin scattering in Titanium Carbide films, *Wave Motion* 68 (2017) 78–87, <https://doi.org/10.1016/j.wavemoti.2016.08.011>.
- [37] A. Trzaskowska, S. Mielcarek, J. Sarkar, Band gap in hypersonic surface phononic lattice of nickel pillars, *J. Appl. Phys.* 114 (2013) 134304, <https://doi.org/10.1063/1.4824103>.
- [38] D. Trung Nguyen, W. Hease, C. Baker, E. Gil-Santos, P. Senellart, A. Lemaitre, S. Ducci, G. Leo, I. Favero, Improved optomechanical disk resonator sitting on a pedestal mechanical shield, *New J. Phys.* 17 (2015) 023016. <https://doi.org/10.1088/1367-2630/17/2/023016>.
- [39] F. Kargar, B. Debnath, J.-P. Kakko, A. Saynatjoki, H. Lipsanen, D.L. Nika, R.K. Lake, A.A. Baladin, Direct observation of confined acoustic phonon polarization branches in free-standing semiconductor nanowires, *Nat. Commun.* 7 (2016) 13400, <https://doi.org/10.1038/ncomms13400>.
- [40] Y. Jin, Y. Pennec, Y. Pan, B. Djafari-Rouhani, Phononic crystal plate with hollow pillars connected by thin bars, *J. Phys. D: Appl. Phys.* 50 (2017) 035301, <https://doi.org/10.1088/1361-6463/50/3/035301>.
- [41] Yan-Feng Wang, Yi-Ze Wang, Bin Wu, Weiqiu Chen, Yue-Sheng Wang, Tunable and Active Phononic Crystals and Metamaterials, *Appl. Mech. Rev.* 72 (2020) 04080, <https://doi.org/10.1115/1.4046222>.